Molecular simulation of the vapor-liquid equilibria of xylene mixtures
Force field performance, and Wolf vs. Ewald for electrostatic interactions

Caro-Ortiz, Sebastián; Hens, Remco; Zuidema, Erik; Rigutto, Marcello; Dubbeldam, David; Vlugt, Thijs J.H.

DOI
10.1016/j.fluid.2018.12.006

Publication date
2019

Document Version
Accepted author manuscript

Published in
Fluid Phase Equilibria

Citation (APA)
Caro-Ortiz, S., Hens, R., Zuidema, E., Rigutto, M., Dubbeldam, D., & Vlugt, T. J. H. (2019). Molecular simulation of the vapor-liquid equilibria of xylene mixtures: Force field performance, and Wolf vs. Ewald for electrostatic interactions. *Fluid Phase Equilibria*, *485*, 239-247. https://doi.org/10.1016/j.fluid.2018.12.006

Molecular Simulation of the Vapor-Liquid Equilibria of Xylene mixtures: Force Field performance, and Wolf vs. Ewald for Electrostatic Interactions

Sebastián Caro-Ortiz[a], Remco Hens[a], Erik Zuidema[b], Marcello Rigutto[b], David Dubbeldam[c], Thijs J. H. Vlugt[a]

[a] *Engineering Thermodynamics, Process & Energy Department, Faculty of Mechanical, Maritime and Materials Engineering, Delft University of Technology, Leeghwaterstraat 39, 2628 CB Delft, The Netherlands*
[b] *Shell Global Solutions International, PO Box 38000, 1030 BN, Amsterdam, The Netherlands*
[c] *Van 't Hoff Institute of Molecular Sciences, University of Amsterdam, Science Park 904, 1098 XH Amsterdam, The Netherlands*

Abstract

This article explores how well vapor-liquid equilibria of pure components and binary mixtures of xylenes can be predicted using different force fields in molecular simulations. The accuracy of the Wolf method and the Ewald summation is evaluated. Monte Carlo simulations in the Gibbs ensemble are performed at conditions comparable to experimental data, using four different force fields. Similar results using the Wolf and the Ewald methods can be obtained for the prediction of densities and the phase compositions of binary mixtures. With the Wolf method, up to 50% less CPU time is used compared to the Ewald method, at the cost of accuracy and additional parameter calibration. The densities of p-xylene and m-xylene can be well estimated using the TraPPE-UA and AUA force fields. The largest differences of VLE with experiments are observed for o-xylene. The p-xylene/o-xylene binary mixtures at 6.66 and 81.3 kPa are simulated, leading to an excellent agreement in the predictions of the composition of the liquid phase compared to experiments. The composition of the vapor phase is dominated by the properties of the component with the largest mole fraction in the liquid phase. The accuracy of the predictions of the phase composition are related to the quality

---

Email address: `t.j.h.vlugt@tudelft.nl` (Thijs J. H. Vlugt)

of the density predictions of the pure component systems. The phase composition of the binary system of xylenes is very sensitive to slight differences in vapor phase density of each xylene isomer, and how well the differences are captured by the force fields.

Keywords: Monte Carlo Simulation, Vapor-Liquid Equilibria, Xylene, Wolf method, Binary mixture

---

1. Introduction

Xylenes are aromatic species that are mainly produced by the catalytic reforming of crude oil, in a mixture usually containing benzene, toluene and xylenes [1]. Further extraction and distillation processes yield equilibrium mixtures of xylenes that generally contain 53% meta-xylene (mX), 24% ortho-xylene (oX) and 23% para-xylene (pX) [2]. Considering the practical application of each component of the mixture, the separation and further transformation of each isomer is important. From the isomers, pX has the highest economic value [3], and is a core raw material for manufacturing polyester fibers [4]. oX is mostly used in the production of phthalic anhydride [5], while the main component of the mixture, mX, has a limited end use and is preferably isomerized into pX or oX [6]. Xylenes are components of solvents, paint thinners, varnish, corrosion preventives and cleaning agents [7].

Separation of xylenes is a challenge [1, 8, 9, 10]. Separation of oX from the mixture can be achieved by distillation, but this is difficult in the mX/pX case due to similar boiling points [11]. It is considered -with the separation of greenhouse gases from dilute emissions and uranium from seawater- as one of the *"seven chemical separation processes to change the world"* [12]. The separation of xylenes on a large scale is performed by the adsorption in porous materials such as X and Y zeolites [13] or by fractional crystallization [14, 15]. Current research efforts are focused on advances of new membranes and sorbents that decrease the energy consumption of such isomer separation [12]. The accurate description and characterization of the thermodynamic properties, such as the vapor-liquid equilibrium (VLE), is critical for the design of proper techniques, equipment, and processes for an efficient separation [16]. Experimental VLE measuremets for xylene mixtures are scarce and only a handful of studies provide data for pure components and binary mixtures of xylenes. For pure component, VLE curves are reported by Smith and Srivastava [17]. For binary mixtures, Rodrigues [18] presented coexistence curves for the pX-mX, pX-oX and mX-oX systems at 100.65 kPa. The pX-mX binary system is described by Kato et al. [19] at atmospheric pressure. Data for 5, 20, 40 and 101.325 kPa is reported by Onken and Arlt [20]. Llopis and Monton [21, 22] reported data for pX-oX and mX-oX systems at 6.66 and 26.66 kPa, Parvez et al. [23] characterized the pX-oX coexistence curves at 81.3 kPa. The coexistence of oX-mX at 298.15K is described by Wichterle et al. [24]. Such studies report that binary mixtures of xylenes have small differences from an ideal mixture [18, 19, 20, 21, 23].

Molecular simulations are an extensively used tool to predict the thermodynamic properties of a wide variety of systems [25]. Fluid phase properties of pure components and mixtures can be computed for large ranges of conditions, even when experiments can be challenging, expensive or dangerous [25]. The Monte Carlo (MC) method in the Gibbs ensemble [26] has been widely used to compute VLE [27, 28, 29, 30, 31, 32, 33]. The choice of a force field that accurately describes the interaction potential between atoms and molecules is a crucial factor. The Gibbs ensemble considers two simulation boxes to simulate the properties of coexisting phases avoiding the vapor-liquid interface [27]. Fig. 1 shows the vapor and liquid phases of a xylene mixture in two separate boxes of a NPT-Gibbs ensemble MC simulation. Molecular simulations of VLE are typically performed employing force fields that model the interactions with Lennard-Jones potentials (LJ) or a combination of LJ and electrostatic interactions. In the case of aromatic compounds, a common practice in the development of the potentials is to fit the interaction parameters to reproduce the VLE of the pure component [34, 35, 36, 37], or by ab initio quantum mechanical calculations [38, 39, 40]. Several force field for xylene interactions have been reported in literature [41, 42, 43, 37, 44, 40], some of which are briefly described in the next section for further use.

The electrostatic interactions are generally represented by charged interaction sites. The Ewald summation method [45] has been extensively used to account these interactions in periodic systems [46]. The electrostatic energy is calculated in two parts by dividing the potential in a short-range contribution computed in real space, and a long-range contribution calculated involving a Fourier transform of the charge density [25]. The long-range contribution constitutes the main disadvantage of the method, it is computationally expensive. Several alternative methods have been developed such as the particle-particle and particle-mesh algorithm [47], the reaction field method [48], the fast multipole algorithm [49], and the Wolf method [50]. These methods are reviewed in depth by Cisneros et al. [51]. From these methods, the Wolf method has been effectively applied to a wide variety of systems [52, 53, 54, 55, 56, 57, 58, 59] and has gained attention due to its efficiency compared to the Ewald method as the Fourier part is not often needed in dense systems. To use this method, the cut-off radius (R_c) and the damping factor (α) have to be determined for each system with the procedures described by Hens and Vlugt [60], and Waibel and Gross [61].

This article explores how the VLE of pure components and binary mixtures of xylenes can be predicted using molecular simulations and how well the Wolf method can be applied. The simulation details such as the input and force fields are summarized in Section 2. The simulation results of VLE for pure components and binary mixtures are analyzed in Section 3. The concluding remarks about force field performance and the use of the Wolf method are discussed in Section 4.

2. Simulation details

The Monte Carlo technique in the Gibbs Ensemble [26] is used for the simulations. The calculations for the VLE of pure components are performed using the Gibbs ensemble at constant total volume (NVT). The isothermal-isobaric version of the Gibbs ensemble (NPT) is used for the binary mixture VLE calculations. The total system contains 1,000 molecules and the interactions between different atom types are calculated using Lorentz-Berthelot mixing rules [62]. The LJ interactions are truncated at 14 Å and analytic tail corrections are applied [62]. The Continuous Fractional Component MC (CFCMC) method in the Gibbs ensemble developed by Poursaeidesfahani et al. [63, 64, 65] is used. The Gibbs ensemble is expanded with one extra molecule -the fractional molecule- per molecule type. The fractional molecules have negligible effect on the thermodynamic properties [64]. The interactions of the fractional molecule are scaled in range 0 to 1 (0 for no interactions with surrounding molecules and 1 for full interaction with surrounding molecules) described by λ. The trial moves in each MC cycle are selected at random within the following fixed probabilities: 33% translation, 33% rotation, 17% changes of the value of λ, 8% identity change of the fractional molecule -where the fractional molecule turns into a whole one, while a molecule in the other box turns into a fractional molecule-, 8% swap move -the fractional molecule is transfered from one box to the other-, and 1%

volume change. All simulations are performed in an in-house developed code which has been verified to yield the same results as the RASPA software [66, 67]. The number of steps per MC cycle is equal to the total number of molecules in the system. Each simulation starts with 5,000 MC cycles to equilibrate the system by only allowing rotation and translation trial moves. After that, a stage of 40,000 MC cycles initializes the system and all types of trial moves are allowed. In this stage, the Wang-Landau algorithm [68] is used to construct a weight function that flattens the probability distribution of λ, so that all values of λ have the same probability, and that the fractional molecule is equally likely to be found in one of the boxes. The chemical potential is calculated from the probability distribution of λ using the procedure described by Poursaeidesfahani et al. [63]. The initialization stage is followed by a production run of 100,000 MC cycles. The reported errors account for the 95% confidence interval calculated by dividing the production run into five sections.

Each simulation starts with a different initial composition (i.e. number of molecules in each box) which is based on the experimental data available for each system. For pure components, the number of molecules and box sizes can be found in the Supporting Information. For binary mixtures, the initial composition can be obtained with the procedure described by Ramdin et al. [27] when experiments are not available. The pX-oX binary mixtures at 6.66 kPa and 81.3 kPa are simulated. The initial guess for the side length of the cubic boxes are 60 Å for the liquid phase box and 145 Å for the vapor phase box. Initially, 920 and 80 molecules are assigned to the liquid and vapor boxes, respectively. The guess for the initial phase compositions of each box are chosen to match the experimental phase compositions [21, 23].

Four different force fields that model the interactions between xylene isomers are used, each one having a particular approach to describe electrostatic interactions. All molecules are defined as rigid and the geometries are according to the original references [41, 34, 42, 37]. The force field parameters are listed in the Supporting Information. The force fields considered are the following:

1. Transferable Potential for Phase Equilibria - United Atom (TraPPE-UA) [41], a widely used force field that is designed to reproduce the VLE of alkylbenzenes as single components. The united atom approach is conveniently used by merging a carbon atom and its bonded hydrogen atoms into a single uncharged interaction site representing each CH_x group in the aromatic species.

2. A modification of the TraPPE-UA force field to include an all-atom approach and charges in the aromatic ring, here called TraPPE-UA-EH. This force field uses the united atom approach from TraPPE-UA [41] to represent the methyl groups, while the bonded carbon and hydrogen atoms from the aromatic ring are individually represented in single interaction centers with charges of -0.95e and +0.95e, respectively [34].

3. Optimized Potential for Liquid Simulations (OPLS) [42, 69], a widely applied force field that represents the aromatic ring with an all atom approach and the methyl group as a carbon centered atom [70]. Each atom has electrostatic charges.

4. Anisotropic United Atom (AUA) [37, 71]. This force field presents a united atom approach, having uncharged single interaction centers for the $\mathrm{CH_x}$ groups and positioning the atom in the direction of the center of mass of the atom group, displacing it from the carbon atom position, unlike the other force fields. One of its main features is the representation of the π-cloud in the aromatic ring. One positive partial charge (+8.13e) in the center of the ring, and two negative partial charges (-4.065e) located at 0.4 Å above and below the plane of the aromatic ring are introduced. The negative charges are displaced from the center of the ring to reproduce the experimental dipole moment of the molecule.

The Ewald summation parameters are chosen such that a relative precision of 10^{-6} is achieved [25]. The Wolf summation parameters are chosen according to the procedure described by Hens and Vlugt [60]. By taking into account the experimental data as a starting point, a short simulation in the NVT ensemble is performed. The chosen density is close to the equilibrium coexistence density. The chosen temperature is above the critical temperature. The system sizes are equal to the initial guess of the box sizes for the binary mixture calculations in the the Gibbs ensemble. From this configuration, the electrostatic energy is calculated for several cut-off radii (R_c) and damping factors (α). This energy can be compared to a reference calculated with the Ewald method for the same system configuration. Following this procedure, it is determined that an optimum parameter set for the vapor phase is: R_c=85 Å, α=0.04 Å^{-1}; and for the liquid phase: R_c=16 Å, α=0.17 Å^{-1}.

3. Results and discussion

3.1. Vapor-liquid equilibria of pure components

The VLE of pure components are calculated with NVT-Gibbs ensemble Monte Carlo simulations using the CFCMC method [63]. Simulations are performed for each isomer using the Ewald and the Wolf methods. The densities for mX are shown in Fig. 2. The calculated coexistence densities for the three isomers with the statistical uncertainties are listed in the Supporting Information. The differences of the use of the Wolf and Ewald methods for pX and oX computed VLEs are qualitatively the same as for mX. The computed VLEs for the TraPPE-UA-EH and AUA show excellent agreement between the Ewald and Wolf methods. The differences in the calculated densities are lower than 1% of the densities and lower than the statistical error of the simulation. The vapor-liquid coexistence densities calculated with the OPLS force field show agreement within the statistical error. The calculated vapor phase densities are underestimated at temperatures between 500 and 550 K using the Wolf method. At high temperatures, the size of the vapor phase box and the number of molecules are different than the values used to determine the optimal damping factor α and cut-off radius (R_c). This suggests that the vapor density of the system is more sensitive to the choice of the Wolf parameters for the OPLS force field than for the other force fields. The chemical potentials as a function of temperature for the two phases of mX using the Wolf method are shown in Fig. 3. The differences in the chemical potential between the phases are within the statistical error. Chemical equilibrium between the vapor and liquid phases is observed as the same chemical potential is calculated for both phases.

The vapor-liquid coexistence curves of mX, oX, and pX calculated using the Ewald method are shown in Fig. 4 for each force field. Clear differences can be observed in Fig. 4 for the density calculations with the experimental data. For mX, the TraPPE-UA and the AUA force field predict liquid densities that deviate up to 3% from the experimental data, while TraPPE-UA-EH and OPLS force fields show significantly higher differences. The experimental liquid densities of pX are well predicted by TraPPE-UA, TraPPE-UA-EH and AUA, as the difference with the computed density is below the statistical error. The OPLS force field shows slightly higher differences of up to 4% at 550 K. The use of the TraPPE-UA force field yields the best prediction of the experimental density of oX. The differences are of the order of two times the statistical uncertainty for the considered temperature range, followed by AUA, with three times the statistical error.

Significantly larger differences than in the liquid phase can be observed in the vapor phase for the simulations and the experimental data. The calculated vapor densities are in agreement with the experiments at low temperatures (i.e. <450 K), and the differences arise at higher temperatures. The vapor densities obtained with the TraPPE-UA and AUA force fields closely follow the experimental data for mX. The highest deviations of the density for every isomer are found with the OPLS force field. The largest differences with the experimental data can be found for the oX vapor density at temperatures over 450 K, where all force fields present deviations larger than the statistical uncertainties from the experimental data. Such differences for oX can be related to assumptions such as having fixed charges, a rigid molecule, and transferable force field parameters for the three isomers. Assuming fixed charges implies a fixed dipole/quadrupole moment. The aromatic π clouds result in a non-negligible quadrupole moment for the aromatic ring [41], which is only considered by the AUA force field. The dipole polarization changes with the temperature, specially for mX and oX [72], which is not considered by any of the force fields.

The critical temperatures (T_c) and critical densities (ρ_c) are extrapolated using the fitting procedure described by Dinpajooh et al. [73]. The obtained critical points of mX, oX and pX for each force field are listed with experimental data in Table 1. In general, the differences between the critical point for each force field using the Wolf and Ewald methods are within the statistical error. This is related to the agreement found for the TraPPE-UA-EH and AUA force fields shown in Fig. 4. However, the different densities obtained at high temperature with the Wolf and the Ewald methods for the OPLS force field have an impact on the determined critical point for xylene isomers. The largest difference of the estimated critical temperature between the Wolf and the Ewald methods is 14 K, for oX using the OPLS force field. The difference of the critical point of the three isomers and the experimental data is smaller than the statistical uncertainties for TraPPE-UA and AUA, as well as the experimental critical point of pX is predicted by all the simulations within the uncertainties.

3.2. Vapor-liquid Equilibria of binary mixtures

The VLE of the pX-oX binary mixture at 6.66 kPa is calculated with NPT-Gibbs ensemble Monte Carlo simulations using the CFCMC method

[63]. The simulations are performed with each force field using the Ewald and the Wolf methods. The phase compositions obtained with the TraPPE-UA-EH, OPLS, and AUA force fields using the Wolf and Ewald methods are shown in Fig. 5. It can be observed that the composition of the liquid phase is not affected by the choice of force field or method for accounting the electrostatic interactions. The statistical uncertainties are larger in the vapor phase than in the liquid phase, and there is a reasonable agreement between the calculated vapor phase compositions with both methods for electrostatic interactions.

The phase diagrams of the pX-oX binary mixture at 6.66 kPa simulated using the Ewald method with experimental data are shown in Fig. 6. Llopis and Monton [21] reported discrete measurements of the phase composition of the mixture. This data is shown as lines to facilitate comparison with the simulations. The experimental uncertainties reported are 0.1 K for the temperature and a standard deviation of 0.001 for reported mole fractions. Small differences from ideality are reported [21] and a small difference between the phase compositions is observed. The experimental data suggests that the vapor does not have the same composition as the liquid. The component with the lowest boiling temperature will have a higher molar fraction in the vapor phase than that with the higher boiling temperature. The simulated composition of the liquid phase is in excellent agreement with the experimental data and the differences are below the statistical uncertainties. Larger differences can be observed for the composition of the vapor phase, where simulations seem to predict an azeotrope behavior, as a phase composition in the vapor equal to the liquid can be found at temperatures between 334 and 336 K. The mole fraction of pX in the vapor phase is higher than in the liquid phase at temperatures higher than 335K, whereas an opposite behavior is predicted by the simulations for temperatures lower than 334 K. This suggests that the vapor phase composition of the component with the highest mole fraction in the liquid phase is underestimated by the simulations. It is important to note that the temperature range of these simulations is out of the fitting range of the force fields, so the observed azeotropic behavior can be an artifact of the force field.

The excess chemical potential of pX in the liquid phase of the pX/oX mixture at 6.66 kPa, as a function of the liquid phase composition is shown in Fig. 7. The reference state for the excess chemical potential is the ideal gas. The excess chemical potential computed for each force field with the Wolf and Ewald methods agree between the statistical uncertainties. A slight increase of the excess chemical potential of pX in the liquid phase can be observed as the mole fraction of pX increases in the mixture. However, this increase is small and within the error bars. The excess chemical potential is directly related to the activity coefficient of the component in the mixture [74, 75]. The activity coefficients for pX reported by the experimental work [21] do not show dependence on the phase composition of the mixture, which is in agreement with the excess chemical potential calculated in the simulations.

The phase diagrams of the pX-oX binary mixture at 81.3 kPa simulated using the Ewald summation for all the force fields and experimental data [23] are shown in Fig. 8. The reported experimental uncertainty for the temperatures is 0.1 K. Small deviations from ideality are reported [23], and a difference between the phase compositions smaller than in the binary mixture at 6.66 kPa can be observed. Larger differences in the computed composition of the liquid phase with the experiments than at 6.66 kPa are found. The prediction of the liquid phase composition obtained using the TraPPE-UA and TraPPE-UA-EH force fields show excellent agreement with experiments. Small deviations from the experimental liquid phase composition are obtained using the OPLS and AUA force fields when the phase composition of oX is higher than for pX. The prediction of the composition of the vapor phase obtained with the TraPPE-UA force field qualitatively predicts the experimental composition of the vapor phase. However, the predictions overestimate the mole fraction of pX in the vapor phase when the mole fraction of oX is larger than for pX in the liquid phase. The simulations with the rest of force fields yield an azeotrope as in the simulations at 6.66 kPa. This suggests that the vapor phase composition of the component with the highest mole fraction in the liquid phase is underestimated by the simulations. It can be concluded that for the tested force fields, the predictions of the composition of the vapor phase are predominantly represented by the properties of the component with the largest mole fraction in the liquid phase. The accuracy of the calculations are related to how well the densities can be calculated for the pure components. The differences on the estimation of the density of oX as a pure component play a significant role in the determination of the VLE of binary mixtures of xylenes.

4. Conclusions

The VLE of xylenes as a single components and binary mixtures have been calculated using the Wolf and Ewald methods. Comparable results using the Wolf and the Ewald methods can be obtained for the prediction of densities and the phase compositions of binary mixtures. With the Wolf method, up to 50% less CPU time is used compared to the Ewald method, at the cost of accuracy and additional parameter calibration. The performance of the considered force fields to predict the VLE of xylene isomers as pure component has been tested. The TraPPE-UA and AUA force fields provide a reasonable estimate of the experimentally determined densities for pX and mX. The largest differences with experimental data are observed in the calculations of the vapor density of oX. The use of the TraPPE-UA force field yields the best prediction of the experimental density of oX. Simulations of pX/oX binary mixtures at 6.66 and 81.3 kPa are in excellent agreement with the experimental data for the liquid phase composition. The predictions of the composition of the vapor phase are dominated by the properties of the component with the highest mole fraction in the liquid phase. The accuracy of the phase composition predictions are related to the quality of the density predictions of the pure component systems. The experimental vapor phase composition is not well predicted by the simulations. This is related to the deviations observed for the prediction of the vapor density of oX as a pure component. For this reason, only a qualitative prediction of the vapor phase composition was obtained using the TraPPE-UA force field for the pX-oX binary mixture at 81.3 kPa. The simulations have shown the potential to accurately predict the phase compositions of such binary mixture, but the development of force fields that predict the VLE of each xylene isomer more accurately -especially oX- is needed. The binary systems of xylenes are very sensitive to the slight density differences in the vapor phase of each xylene isomer and how well these are captured by the force fields.

Acknowledgements

This work was sponsored by NWO Exacte Wetenschappen (Physical Sciences) for the use of supercomputer facilities, with financial support from the Nederlandse Organisatie voor Wetenschappelijk Onderzoek (Netherlands Organization for Scientific Research, NWO). T.J.H.V. acknowledges NWO-CW for a VICI grant. The authors also gratefully acknowledge financial support from Shell Global Solutions B.V.

Table 1: Critical temperatures (T_c) and critical densities (ρ_c) of pure components extrapolated from VLE simulations using the fitting procedure described by Dinpajooh et al. [73]. (E) and (W) denote the use of the Ewald and the Wolf methods, respectively. The numbers between round brackets denote the uncertainty in the last digit. Experimental data are from Refs. [76, 77, 78].

	m-xylene		o-xylene		p-xylene	
T_c/[K], ρ_c/[kg/m^3]	T_c	ρ_c	T_c	ρ_c	T_c	ρ_c
Experimental [76, 77, 78]	616.4(10)	283(4)	630.5(10)	287(4)	617.6(10)	281(4)
TraPPE-UA	620(7)	288(7)	629(7)	297(6)	617(4)	286(8)
TraPPE-UA-EH (E)	604(11)	279(7)	622(6)	278(5)	626(9)	279(6)
TraPPE-UA-EH (W)	610(9)	270(6)	623(5)	275(3)	620(7)	278(7)
OPLS (E)	605(9)	290(9)	626(8)	293(6)	609(8)	285(6)
OPLS (W)	609(9)	279(5)	612(9)	300(9)	611(9)	277(8)
AUA (E)	618(9)	284(6)	625(9)	293(6)	616(8)	290(6)
AUA (W)	618(9)	281(7)	627(8)	286(7)	616(14)	288(8)

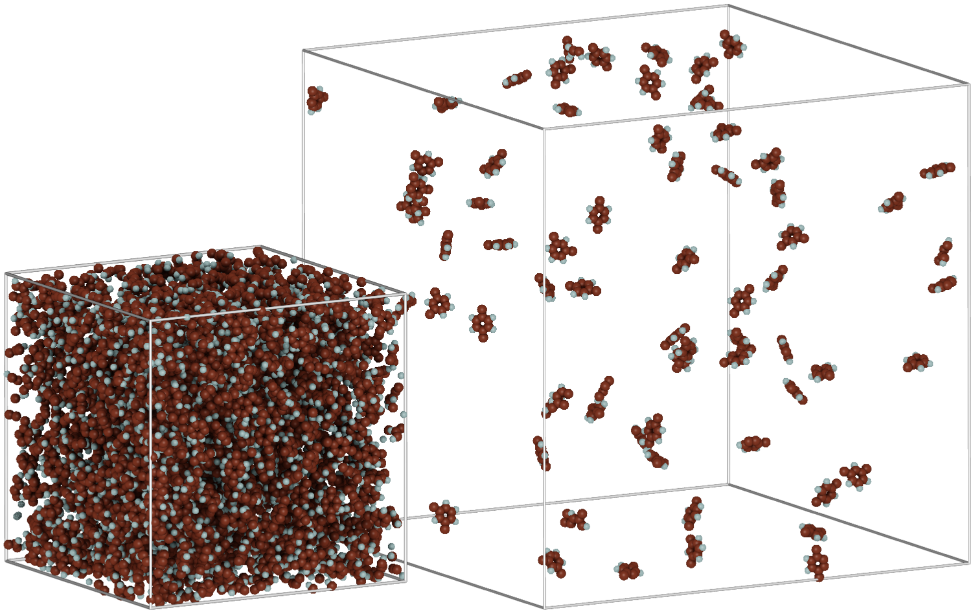

Figure 1: Schematic representation of the NPT-Gibbs Ensemble MC simulation of the pX-mX binary mixture. The two boxes represent the liquid (left) and vapor (right) phases. Figure rendered with the iRASPA visualization software [79].

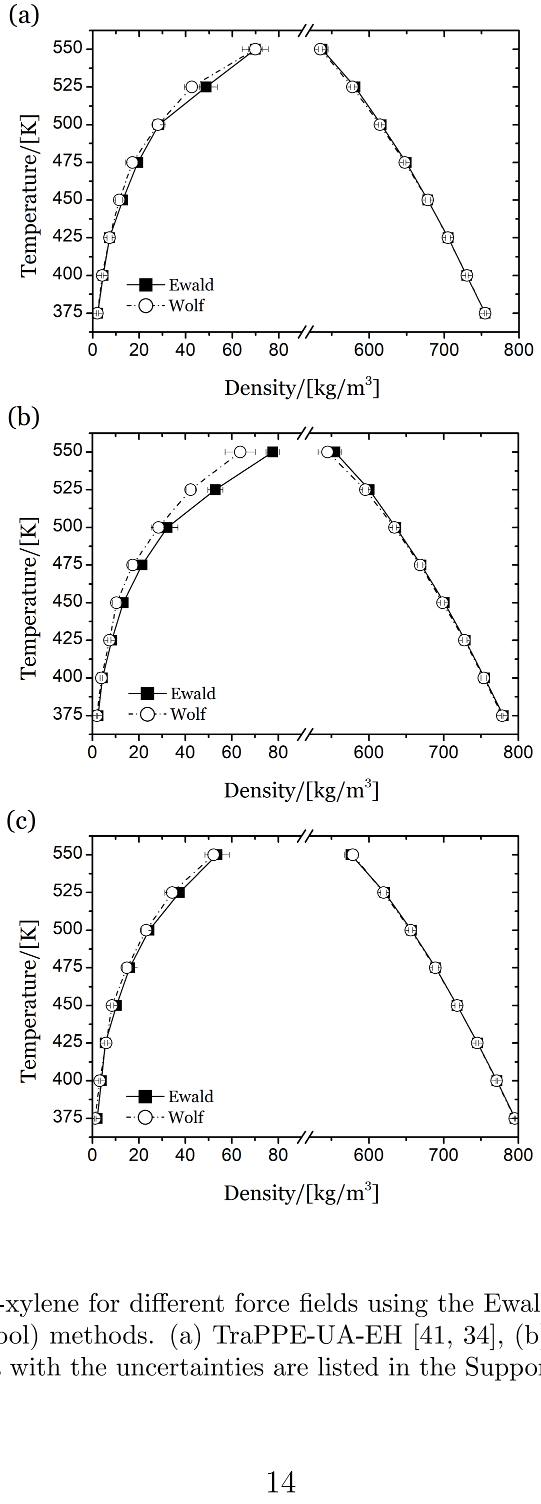

Figure 2: VLE of m-xylene for different force fields using the Ewald (closed symbol) and the Wolf (open symbol) methods. (a) TraPPE-UA-EH [41, 34], (b) OPLS [42], (c) AUA [37]. Tabulated data with the uncertainties are listed in the Supporting Information.

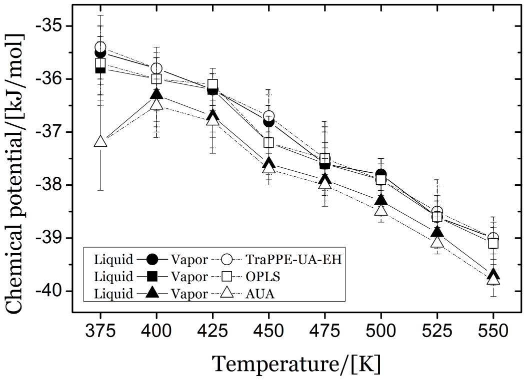

Figure 3: Chemical potential of m-xylene at VLE coexistence as a function of temperature using the Wolf method for each force field. Closed and open symbols represent the liquid and vapor boxes, respectively. Tabulated data with the uncertainties are listed in the Supporting Information.

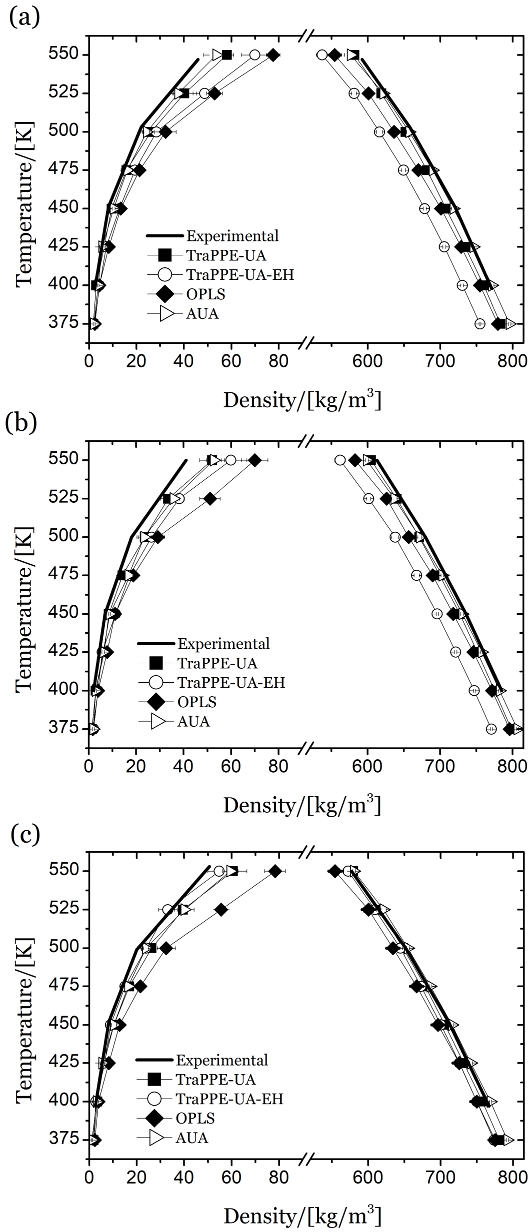

Figure 4: Vapor-liquid equilibria of (a) m-xylene, (b) o-xylene, and (c) p-xylene for each force field using the Ewald summation method. Experimental data from Ref. [17] is also included. Tabulated data with the uncertainties are listed in the Supporting Information.

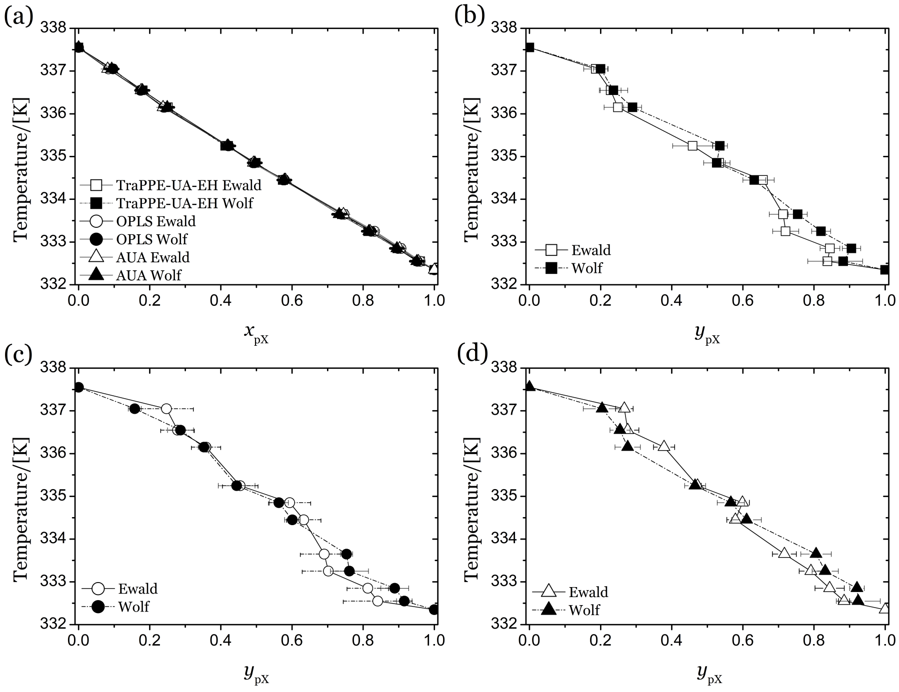

Figure 5: Phase composition diagrams of the p-xylene/o-xylene binary mixture at 6.66 kPa using the Wolf and Ewald methods. (a) Liquid phase composition for TraPPE-UA-EH [41, 34], OPLS [42] and AUA [37] force fields. Vapor phase composition for (b) TraPPE-UA-EH [41, 34], (c) OPLS [42], and (d) AUA [37]. x_{pX} is the mole fraction of pX in the liquid phase. y_{pX} is the mole fraction of pX in the vapor phase. Closed and open symbols represent the values using the Wolf and the Ewald method, respectively. Tabulated data with the uncertainties are listed in the Supporting Information.

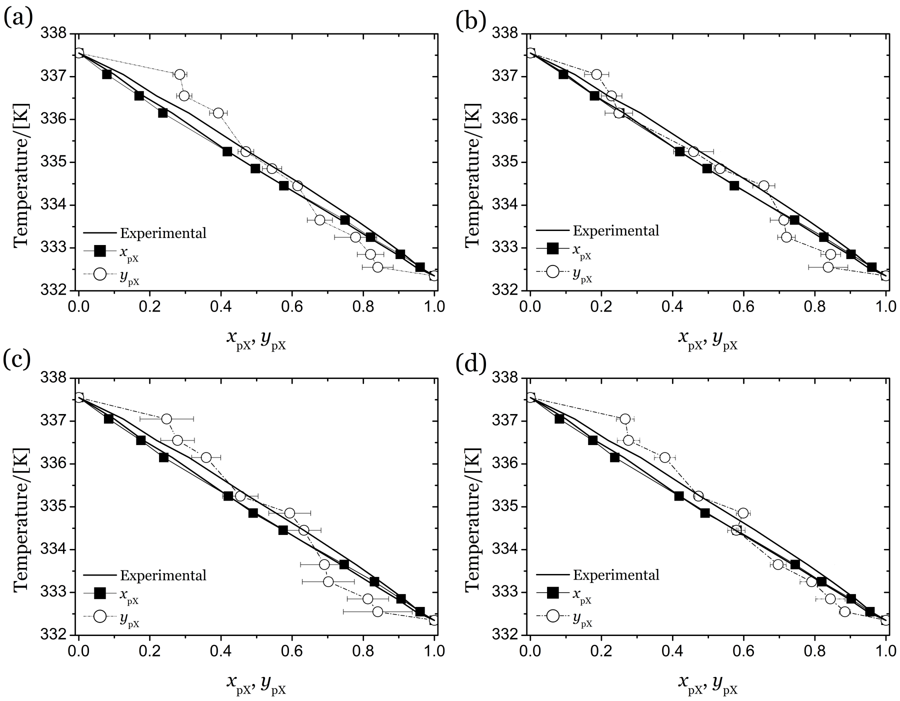

Figure 6: Phase diagram of the p-xylene/o-xylene binary mixture at 6.66 kPa for (a) TraPPE-UA [41], (b) TraPPE-UA-EH [41, 34], (c) OPLS [42], and (d) AUA [37], calculated using the Ewald method. Experimental data are from Llopis and Monton [21]. x_{pX} (closed symbols) is the mole fraction of pX in the liquid phase. y_{pX} (open symbols) is the mole fraction of pX in the vapor phase. Tabulated data with the uncertainties are listed in the Supporting Information.

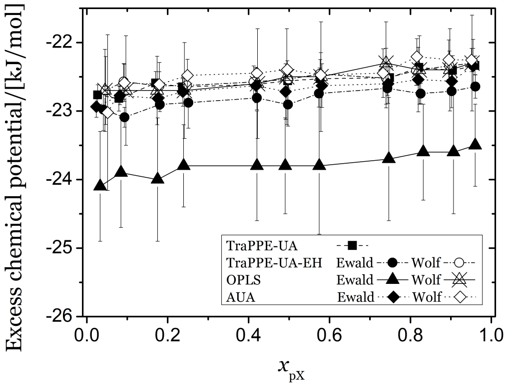

Figure 7: Excess chemical potential ($\mu^{\mathrm{e}}{}_{\mathrm{pX}}$) of p-xylene in the liquid phase of the pX/oX binary mixture at 6.66 kPa, as a function of the liquid phase composition for all force fields. Closed and open symbols denote the use of the Ewald and the Wolf methods, respectively. Tabulated data with the uncertainties are listed in the Supporting Information.

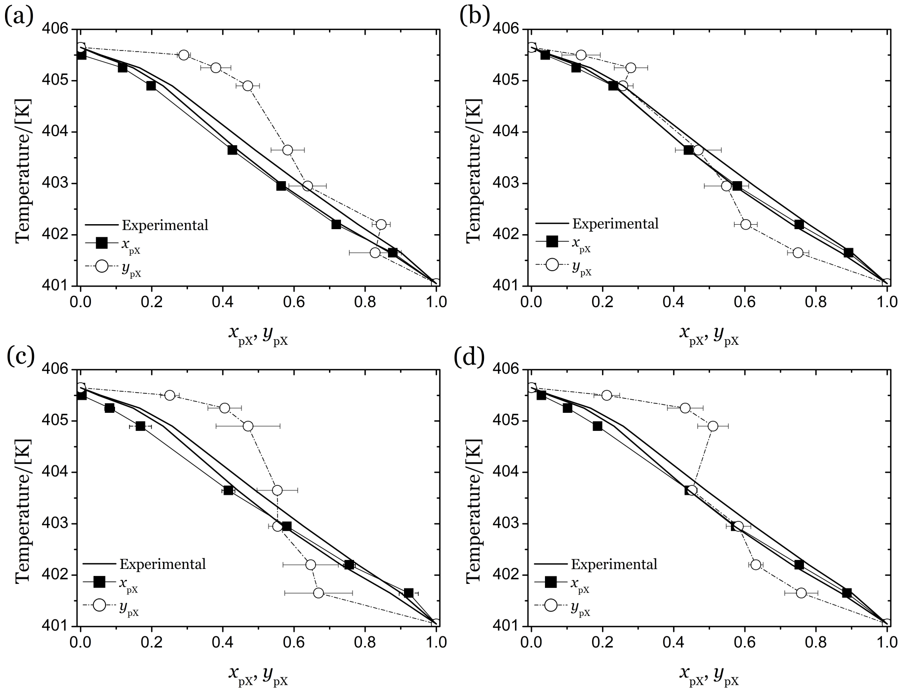

Figure 8: Phase diagram of the p-xylene/o-xylene binary mixture at 81.3 kPa for (a) TraPPE-UA [41], (b) TraPPE-UA-EH [41, 34], (c) OPLS [42], and (d) AUA [37], calculated using the Ewald method. Experimental data are from Parvez et al [23]. x_{pX} (closed symbols) is the mole fraction of pX in the liquid phase. y_{pX} (open symbols) is the mole fraction of pX in the vapor phase. Tabulated data with the uncertainties are listed in the Supporting Information.

5. References

[1] Y. Yang, P. Bai, X. Guo, Separation of Xylene Isomers: A Review of Recent Advances in Materials, Industrial & Engineering Chemistry Research 56 (2017) 14725–14753.

[2] J. Das, Y. Bhat, A. Halgeri, Aromatization of C_4-C_6 hydrocarbons to benzene, toluene and para xylene over pore size controlled ZnO-HZSM-5 zeolite, in: T. S. R. P. Rao, G. M. Dhar (Eds.), Recent Advances In Basic and Applied Aspects of Industrial Catalysis, volume 113 of *Studies in Surface Science and Catalysis*, Elsevier, 1998, pp. 447 – 453.

[3] C. J. Egan, R. V. Luthy, Separation of Xylenes, Industrial & Engineering Chemistry 47 (1955) 250–253.

[4] R. A. F. Tomás, J. C. M. Bordado, J. F. P. Gomes, p-Xylene Oxidation to Terephthalic Acid: A Literature Review Oriented toward Process Optimization and Development, Chemical Reviews 113 (2013) 7421–7469.

[5] M. Minceva, A. Rodrigues, Adsorption of Xylenes on Faujasite-Type Zeolite: Equilibrium and Kinetics in Batch Adsorber, Chemical Engineering Research and Design 82 (2004) 667 – 681.

[6] W. J. Cannella, Xylenes and ethylbenzene, in: Kirk-Othmer Encyclopedia of Chemical Technology, American Cancer Society, 2007.

[7] D. Stoye, W. Freitag, Paints, Coatings and Solvents, Wiley-Blackwell, 2nd edition, 2007.

[8] Z.-Y. Gu, X.-P. Yan, Metal-Organic Framework MIL-101 for High-Resolution Gas-Chromatographic Separation of Xylene Isomers and Ethylbenzene, Angewandte Chemie International Edition 49 (2010) 1477–1480.

[9] M. T. Ashraf, R. Chebbi, N. A. Darwish, Process of p-Xylene Production by Highly Selective Methylation of Toluene, Industrial & Engineering Chemistry Research 52 (2013) 13730–13737.

[10] Y. Ma, F. Zhang, S. Yang, R. P. Lively, Evidence for entropic diffusion selection of xylene isomers in carbon molecular sieve membranes, Journal of Membrane Science 564 (2018) 404 – 414.

[11] Y. Zhou, J. Wu, E. W. Lemmon, Thermodynamic Properties of o-Xylene, m-Xylene, p-Xylene, and Ethylbenzene, Journal of Physical and Chemical Reference Data 41 (2012) 023103.

[12] D. S. Sholl, R. P. Lively, Seven chemical separations to change the world, Nature 532 (2016) 435–437.

[13] A. E. Rodrigues, C. Pereira, M. Minceva, L. S. Pais, A. M. Ribeiro, A. Ribeiro, M. Silva, N. Graa, J. C. Santos, Chapter 5 - The Parex Process for the Separation of p-Xylene, in: A. E. Rodrigues, C. Pereira, M. Minceva, L. S. Pais, A. M. Ribeiro, A. Ribeiro, M. Silva, N. Graa, J. C. Santos (Eds.), Simulated Moving Bed Technology, Butterworth-Heinemann, Oxford, 2015, pp. 117 – 144.

[14] S. R. Dey, K. M. Ng, Fractional crystallization: Design alternatives and tradeoffs, AIChE Journal 41 (1995) 2427–2438.

[15] H. Mohameed, B. A. Jdayil, K. Takrouri, Separation of para-xylene from xylene mixture via crystallization, Chemical Engineering and Processing: Process Intensification 46 (2007) 25 – 36.

[16] M. O. Daramola, A. J. Burger, M. Pera-Titus, A. Giroir-Fendler, S. Miachon, J.-A. Dalmon, L. Lorenzen, Separation and isomerization of xylenes using zeolite membranes: a short overview, Asia-Pacific Journal of Chemical Engineering 5 (2010) 815–837.

[17] B. D. Smith, R. Srivastava, Thermodynamic data for pure compound: Part A, Hydrocarbons and Ketones, Elsevier, Amsterdam, 1986.

[18] W. Rodrigues, S. Mattedi, J. C. N. Abreu, Experimental vapor-liquid equilibria data for binary mixtures of xylene isomers, Brazilian Journal of Chemical Engineering 22 (2005) 453 – 462.

[19] M. Kato, T. Sato, M. Hirata, Vapor-liquid equilibrium relationship of para-xylene meta-xylene system at atmospheric pressure, Journal of Chemical Engineering of Japan 4 (1971) 305–308.

[20] U. Onken, W. Arlt, Recommended test mixtures for distillation columns, IChemE, 2nd edition, 1990.

[21] F. J. Llopis, J. B. Monton, Isobaric vapor-liquid equilibria of p-xylene + o-xylene and m-xylene + o-xylene systems at 6.66 and 26.66 kPa, Journal of Chemical & Engineering Data 39 (1994) 53–55.

[22] F. J. Llopis, J. B. Monton, Isobaric Vapor-Liquid Equilibria for Binary and Ternary Systems Composed of 1,4-Dimethylbenzene, 1,3-Dimethylbenzene, and 1,2-Dimethylbenzene at 6.66 and 26.66 kPa, Journal of Chemical & Engineering Data 39 (1994) 643–646.

[23] M. Parvez, G. Singh, S. Tyagi, S. Kumar, S. Khan, Experimental determination of vapour-liquid equilibrium data for the binary mixtures P-Xylene and O-Xylene at 81.3 kPa, Journal of Scientific and Technical Advancements 1 (2015) 263–265.

[24] I. Wichterle, J. Linek, Z. Wagner, J.-C. Fontaine, K. Sosnkowska-Kehiaian, H. Kehiaian, Vapor-Liquid Equilibrium of the Mixture C_8H_{10} + C_8H_{10} (LB3761, EVLM 1211), in: H. Kehiaian (Ed.), Binary Liquid Systems of Nonelectrolytes. Part 2, Springer Berlin Heidelberg, Berlin, Heidelberg, 2008, pp. 1221–1222.

[25] D. Frenkel, B. Smit, Understanding Molecular Simulation, Academic Press, 2nd edition, 2002.

[26] A. Z. Panagiotopoulos, M. R. Stapleton, The Gibbs method for molecular-based computer simulations of phase equilibria, Fluid Phase Equilibria 53 (1989) 133 – 141. Proceedings of the Fifth International Conference.

[27] M. Ramdin, S. H. Jamali, T. M. Becker, T. J. H. Vlugt, Gibbs ensemble Monte Carlo simulations of multicomponent natural gas mixtures, Molecular Simulation 44 (2018) 377–383.

[28] A. Panagiotopoulos, N. Quirke, M. Stapleton, D. Tildesley, Phase equilibria by simulation in the Gibbs ensemble, Molecular Physics 63 (1988) 527–545.

[29] A. D. Cortés Morales, I. G. Economou, C. J. Peters, J. I. Siepmann, Influence of simulation protocols on the efficiency of Gibbs ensemble Monte Carlo simulations, Molecular Simulation 39 (2013) 1135–1142.

[30] M. Ramdin, T. M. Becker, S. H. Jamali, M. Wang, T. J. H. Vlugt, Computing equation of state parameters of gases from Monte Carlo simulations, Fluid Phase Equilibria 428 (2016) 174 – 181.

[31] P. Ungerer, C. Nieto-Draghi, B. Rousseau, G. Ahunbay, V. Lachet, Molecular simulation of the thermophysical properties of fluids: From understanding toward quantitative predictions, Journal of Molecular Liquids 134 (2007) 71 – 89.

[32] P. Ungerer, B. Tavitian, A. Boutin, Applications of Molecular Simulation in the Oil and Gas Industry - Monte-Carlo Methods, Editions Technip, 1st edition, 2005.

[33] A. Torres-Knoop, N. C. Burtch, A. Poursaeidesfahani, S. P. Balaji, R. Kools, F. X. Smit, K. S. Walton, T. J. Vlugt, D. Dubbeldam, Optimization of Particle Transfers in the Gibbs Ensemble for Systems with Strong and Directional Interactions Using CBMC, CFCMC, and CB/CFCMC, Journal of Physical Chemistry C 120 (2016) 9148–9159.

[34] N. Rai, J. I. Siepmann, Transferable Potentials for Phase Equilibria. 9. Explicit Hydrogen Description of Benzene and Five-Membered and Six-Membered Heterocyclic Aromatic Compounds, Journal of Physical Chemistry B 111 (2007) 10790–10799.

[35] N. Rai, J. I. Siepmann, Transferable Potentials for Phase Equilibria. 10. Explicit-Hydrogen Description of Substituted Benzenes and Polycyclic Aromatic Compounds, Journal of Physical Chemistry B 117 (2013) 273–288.

[36] P. Bonnaud, C. Nieto-Draghi, P. Ungerer, Anisotropic United Atom Model Including the Electrostatic Interactions of Benzene, The Journal of Physical Chemistry B 111 (2007) 3730–3741.

[37] C. Nieto-Draghi, P. Bonnaud, P. Ungerer, Anisotropic United Atom Model Including the Electrostatic Interactions of Methylbenzenes. I. Thermodynamic and Structural Properties, Journal of Physical Chemistry C 111 (2007) 15686–15699.

[38] I. Cacelli, G. Cinacchi, G. Prampolini, A. Tani, Computer Simulation of Solid and Liquid Benzene with an Atomistic Interaction Potential

Derived from ab Initio Calculations, Journal of the American Chemical Society 126 (2004) 14278–14286.

[39] P. E. M. Lopes, G. Lamoureux, B. Roux, A. D. MacKerell, Polarizable Empirical Force Field for Aromatic Compounds Based on the Classical Drude Oscillator, Journal of Physical Chemistry B 111 (2007) 2873–2885.

[40] H. Sun, COMPASS: An ab Initio Force-Field Optimized for Condensed-Phase Applications - Overview with Details on Alkane and Benzene Compounds, Journal of Physical Chemistry B 102 (1998) 7338–7364.

[41] C. D. Wick, M. G. Martin, J. I. Siepmann, Transferable Potentials for Phase Equilibria. 4. United-Atom Description of Linear and Branched Alkenes and Alkylbenzenes, Journal of Physical Chemistry B 104 (2000) 8008–8016.

[42] W. L. Jorgensen, E. R. Laird, T. B. Nguyen, J. Tirado-Rives, Monte Carlo simulations of pure liquid substituted benzenes with OPLS potential functions, Journal of Computational Chemistry 14 (1993) 206–215.

[43] A. K. Rappe, C. J. Casewit, K. S. Colwell, W. A. Goddard, W. M. Skiff, UFF, a full periodic table force field for molecular mechanics and molecular dynamics simulations, Journal of the American Chemical Society 114 (1992) 10024–10035.

[44] K. Chenoweth, A. C. T. van Duin, W. A. Goddard, ReaxFF Reactive Force Field for Molecular Dynamics Simulations of Hydrocarbon Oxidation, Journal of Physical Chemistry A 112 (2008) 1040–1053.

[45] P. P. Ewald, Die Berechnung optischer und elektrostatischer Gitterpotentiale, Annalen der Physik 369 (1921) 253–287.

[46] B. A. Wells, A. L. Chaffee, Ewald Summation for Molecular Simulations, Journal of Chemical Theory and Computation 11 (2015) 3684–3695.

[47] J. W. Eastwood, R. W. Hockney, D. N. Lawrence, P3M3DP The three-dimensional periodic particle-particle/particle-mesh program, Computer Physics Communications 19 (1980) 215 – 261.

[48] L. Onsager, Electric Moments of Molecules in Liquids, Journal of the American Chemical Society 58 (1936) 1486–1493.

[49] L. Greengard, V. Rokhlin, A fast algorithm for particle simulations, Journal of Computational Physics 73 (1987) 325 – 348.

[50] D. Wolf, P. Keblinski, S. R. Phillpot, J. Eggebrecht, Exact method for the simulation of Coulombic systems by spherically truncated, pairwise r^1 summation, Journal of Chemical Physics 110 (1999) 8254–8282.

[51] A. Cisneros, M. Karttunen, P. Ren, C. Sagui, Classical Electrostatics for Biomolecular Simulations, Chemical Reviews 114 (2014) 779–814.

[52] G. S. Fanourgakis, An Extension of Wolf's Method for the Treatment of Electrostatic Interactions: Application to Liquid Water and Aqueous Solutions, Journal of Physical Chemistry B 119 (2015) 1974–1985.

[53] P. Demontis, S. Spanu, G. B. Suffritti, Application of the Wolf method for the evaluation of Coulombic interactions to complex condensed matter systems: Aluminosilicates and water, Journal of Chemical Physics 114 (2001) 7980–7988.

[54] C. Avendaño, A. Gil-Villegas, Monte Carlo simulations of primitive models for ionic systems using the Wolf method, Molecular Physics 104 (2006) 1475–1486.

[55] P. X. Viveros-Méndez, A. Gil-Villegas, Computer simulation of sedimentation of ionic systems using the Wolf method, Journal of Chemical Physics 136 (2012) 154507.

[56] D. Zahn, B. Schilling, S. M. Kast, Enhancement of the Wolf Damped Coulomb Potential: Static, Dynamic, and Dielectric Properties of Liquid Water from Molecular Simulation, Journal of Physical Chemistry B 106 (2002) 10725–10732.

[57] C. J. Fennell, J. D. Gezelter, Is the Ewald summation still necessary? Pairwise alternatives to the accepted standard for long-range electrostatics, Journal of Chemical Physics 124 (2006) 234104.

[58] J. Kolafa, F. Močka, I. Nezbeda, Handling Electrostatic Interactions in Molecular Simulations: A systematic study, Collection of Czechoslovak Chemical Communications 73 (2008) 481–506.

[59] A. Rahbari, R. Hens, S. H. Jamali, M. Ramdin, D. Dubbeldam, T. J. H. Vlugt, Effect of truncating electrostatic interactions on predicting thermodynamic properties of water-methanol systems, Molecular Simulation (2018).

[60] R. Hens, T. J. H. Vlugt, Molecular Simulation of Vapor-liquid Equilibria Using the Wolf Method for Electrostatic Interactions, Journal of Chemical & Engineering Data 63 (2018) 1096–1102.

[61] C. Waibel, J. Gross, Modification of the Wolf Method and Evaluation for Molecular Simulation of Vapor Liquid Equilibria, Journal of Chemical Theory and Computation 14 (2018) 2198–2206.

[62] M. P. Allen, D. Tildesley, Computer Simulation of liquids, Oxford University Press, 2nd edition, 2017.

[63] A. Poursaeidesfahani, A. Torres-Knoop, D. Dubbeldam, T. J. H. Vlugt, Direct Free Energy Calculation in the Continuous Fractional Component Gibbs Ensemble, Journal of Chemical Theory and Computation 12 (2016) 1481–1490.

[64] A. Poursaeidesfahani, A. Rahbari, A. Torres-Knoop, D. Dubbeldam, T. J. H. Vlugt, Computation of thermodynamic properties in the continuous fractional component Monte Carlo Gibbs ensemble, Molecular Simulation 43 (2017) 189–195.

[65] A. Rahbari, R. Hens, I. K. Nikolaidis, A. Poursaeidesfahani, M. Ramdin, I. G. Economou, O. A. Moultos, D. Dubbeldam, T. J. H. Vlugt, Computation of partial molar properties using continuous fractional component Monte Carlo, Molecular Physics 116 (2018) 3331–3344.

[66] D. Dubbeldam, S. Calero, D. E. Ellis, R. Q. Snurr, RASPA: molecular simulation software for adsorption and diffusion in flexible nanoporous materials, Molecular Simulation 42 (2016) 81–101.

[67] D. Dubbeldam, A. Torres-Knoop, K. S. Walton, On the inner workings of Monte Carlo codes, Molecular Simulation 39 (2013) 1253–1292.

[68] F. Wang, D. P. Landau, Efficient, Multiple-Range Random Walk Algorithm to Calculate the Density of States, Physical Review Letters 86 (2001) 2050–2053.

[69] W. L. Jorgensen, D. S. Maxwell, J. Tirado-Rives, Development and Testing of the OPLS All-Atom Force Field on Conformational Energetics and Properties of Organic Liquids, Journal of the American Chemical Society 118 (1996) 11225–11236.

[70] J. M. Castillo, T. J. H. Vlugt, S. Calero, Molecular Simulation Study on the Separation of Xylene Isomers in MIL-47 Metal-Organic Frameworks, Journal of Physical Chemistry C 113 (2009) 20869–20874.

[71] C. Nieto-Draghi, P. Bonnaud, P. Ungerer, Anisotropic United Atom Model Including the Electrostatic Interactions of Methylbenzenes. II. Transport Properties, Journal of Physical Chemistry C 111 (2007) 15942–15951.

[72] H. Kanai, V. Inouye, L. Yazawa, R. Goo, H. Wakatsuki, Importance of Debye and Keesom interactions in separating m-xylene and p-xylene in GC-MS analysis utilizing PEG stationary phase, Journal of Chromatographic Science 43 (2005) 57–62.

[73] M. Dinpajooh, P. Bai, D. A. Allan, J. I. Siepmann, Accurate and precise determination of critical properties from Gibbs ensemble Monte Carlo simulations, Journal of Chemical Physics 143 (2015) 114113.

[74] S. Hempel, J. Fischer, D. Paschek, G. Sadowski, Activity Coefficients of Complex Molecules by Molecular Simulation and Gibbs-Duhem Integration, Soft Materials 10 (2012) 26–41.

[75] S. P. Balaji, S. K. Schnell, E. S. McGarrity, T. J. H. Vlugt, A direct method for calculating thermodynamic factors for liquid mixtures using the Permuted Widom test particle insertion method, Molecular Physics 111 (2013) 287–296.

[76] R. D. Chirico, S. E. Knipmeyer, A. Nguyen, J. W. Reynolds, W. V. Steele, Thermodynamic Equilibria in Xylene Isomerization. 2. The Thermodynamic Properties of m-Xylene, Journal of Chemical & Engineering Data 42 (1997) 475–487.

[77] R. D. Chirico, S. E. Knipmeyer, A. Nguyen, A. B. Cowell, J. W. Reynolds, W. V. Steele, Thermodynamic Equilibria in Xylene Isomerization. 3. The Thermodynamic Properties of o-Xylene, Journal of Chemical & Engineering Data 42 (1997) 758–771.

[78] R. D. Chirico, S. E. Knipmeyer, A. Nguyen, W. V. Steele, Thermodynamic Equilibria in Xylene Isomerization. 1. The Thermodynamic Properties of p-Xylene, Journal of Chemical & Engineering Data 42 (1997) 248–261.

[79] D. Dubbeldam, S. Calero, T. J. H. Vlugt, iRASPA: GPU-accelerated visualization software for materials scientists, Molecular Simulation 44 (2018) 653–676.

Graphical Abstract

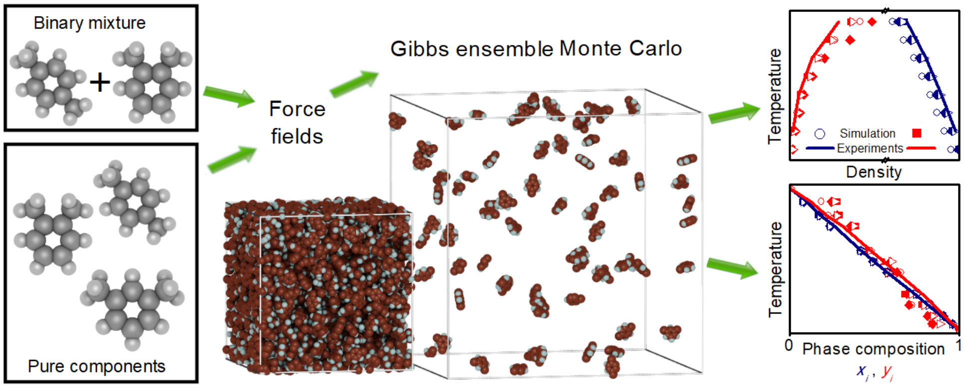

Supporting Information

Molecular Simulation of the Vapor-Liquid Equilibria of Xylene mixtures: Force Field performance, and Wolf vs. Ewald for Electrostatic Interactions

Sebastián Caro-Ortiz[a], Remco Hens[a], Erik Zuidema[b], Marcello Rigutto[b], David Dubbeldam[c], and Thijs J. H. Vlugt[a*]

[a]*Engineering Thermodynamics, Process & Energy Department, Faculty of Mechanical, Maritime and Materials Engineering, Delft University of Technology Leeghwaterstraat 39, 2628 CB Delft, The Netherlands.*

[b]*Shell Global Solutions International, PO Box 38000, 1030 BN, Amsterdam, The Netherlands.*

[c]*Van 't Hoff Institute of Molecular Sciences, University of Amsterdam, Science Park 904, 1098 XH Amsterdam, The Netherlands.*

E-mail: t.j.h.vlugt@tudelft.nl

Table S1: Force field parameters for xylene isomers. All molecules are considered as rigid. For the atom positions, the reader is referred to the original publications of the force fields[1–6].

Force field	Atom	ϵ/k_{B} /[K]	σ/[Å]	q/[e]
TraPPE-UA[1]	C	21.00	3.880	0
	CH	50.50	3.695	0
	CH_3	98.00	3.750	0
TraPPEE-UA-EH[1,2]	C	30.70	3.600	-0.095
	C*	21.00	3.880	0
	H	25.50	2.360	0.095
	CH_3	98.00	3.750	0
OPLS[3,4]	C	35.24	3.550	-0.115
	H	15.03	2.420	0.115
	CH_3	85.51	3.800	0.115
AUA[5,6]	C	35.43	3.361	0
	CH	75.60	3.361	0
	CH_3	120.15	3.607	0
	Center site (+)	0	0	8.130
	π-site (-)	0	0	-4.065

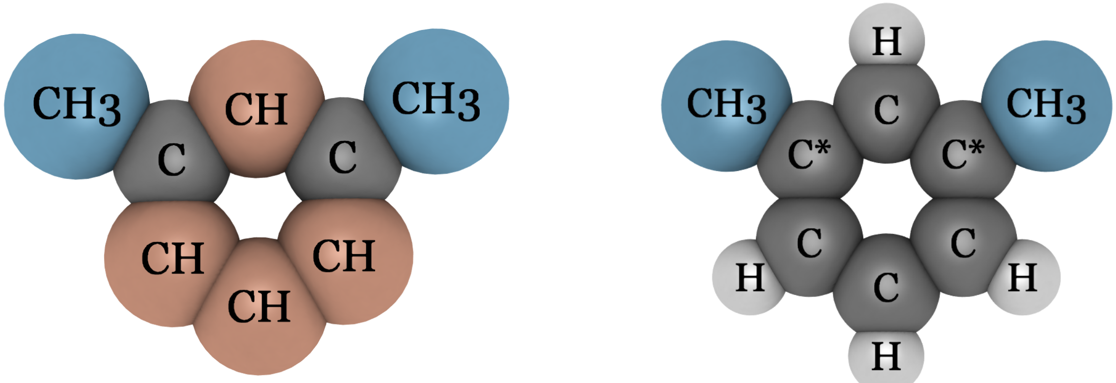

(a) TraPPE-UA

(b) TraPPE-UA-EH

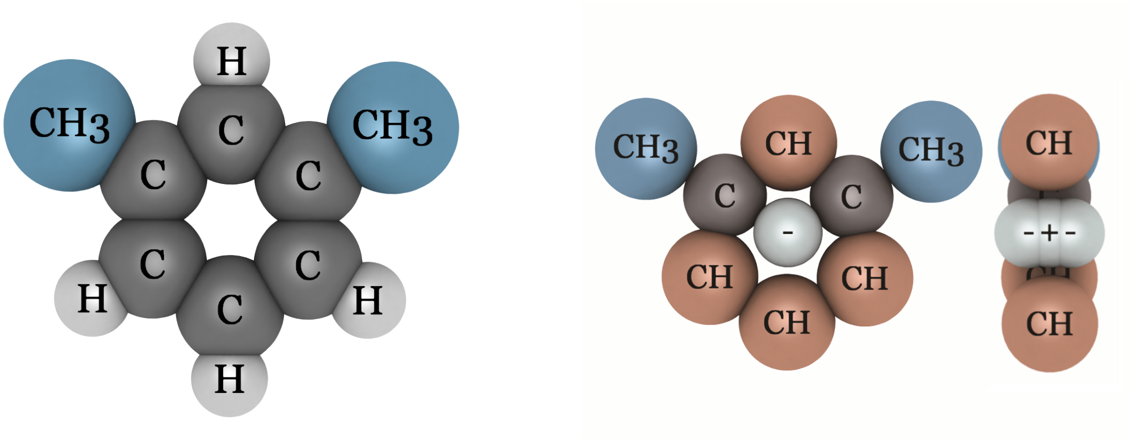

(c) OPLS

(d) AUA

Figure 1: Schematic representation of m-xylene for the (a) TraPPE-UA[1], (b) TraPPE-UA-EH[1,2], (c) OPLS[3,4], and (d) AUA[5,6] force fields. Atom labels use the notation of Table S1. Figure rendered with the iRASPA visualization software[7].

Table S2: VLE simulation input for m-xylene, o-xylene and p-xylene. T is the temperature, N the number of molecules, L the initial length of one side of the (cubic) simulation box. The subscripts l and v indicate the liquid and vapor boxes, respectively.

T/[K]	N_l	N_v	L_l/[Å]	L_v/[Å]
375	965	35	60	142
400	933	67	60	142
425	899	101	60	130
450	863	137	60	126
475	830	170	60	114
500	797	203	60	112
525	760	240	60	112
550	745	255	60	105

Table S3: VLE simulation results for liquid densities (ρ_l) and vapor densities (ρ_v) of m-xylene, o-xylene, and p-xylene for different temperatures (T) obtained with the TraPPE-UA force field. The numbers between round brackets denote the uncertainties in the last digit.

	m-xylene		o-xylene		p-xylene	
T/[K]	ρ_l/[kg/m^3]	ρ_v/[kg/m^3]	ρ_l/[kg/m^3]	ρ_v/[kg/m^3]	ρ_l/[kg/m^3]	ρ_v/[kg/m^3]
375	783(1)	1.8(3)	799(1)	1.4(2)	781(2)	1.8(5)
400	760(1)	3.1(1)	775(2)	2.9(6)	758(2)	3.4(5)
425	734(1)	6.3(11)	752(2)	6.5(7)	732(2)	6.2(7)
450	708(3)	9.5(8)	727(3)	8.4(12)	706(2)	10.4(7)
475	682(2)	16(2)	699(4)	14(2)	679(1)	17(4)
500	652(4)	26(4)	671(2)	24(3)	648(4)	26(2)
525	618(3)	40(5)	640(1)	34(3)	615(4)	39(2)
550	581(3)	58(3)	605(3)	52(5)	579(5)	61(6)

Table S4: VLE simulation results for liquid densities (ρ_l) and vapor densities (ρ_v) of m-xylene, o-xylene, and p-xylene for different temperatures (T) obtained with the TraPPE-UA-EH force field using the Ewald and the Wolf methods. The numbers between round brackets denote the uncertainties in the last digit.

Ewald	m-xylene		o-xylene		p-xylene	
T/[K]	ρ_l/[kg/m^3]	ρ_v/[kg/m^3]	ρ_l/[kg/m^3]	ρ_v/[kg/m^3]	ρ_l/[kg/m^3]	ρ_v/[kg/m^3]
375	755(1)	2.2(4)	771(2)	2.0(2)	774(2)	1.7(4)
400	730(2)	4.5(3)	747(2)	3.8(5)	750(2)	2.8(5)
425	706(2)	7.2(9)	722(2)	6(2)	726(2)	6.5(7)
450	678(2)	13(2)	696(2)	11(1)	700(2)	9(1)
475	649(3)	19(1)	668(4)	17(2)	673(1)	15(2)
500	616(5)	28(3)	638(5)	27(3)	644(4)	24(3)
525	581(3)	49(5)	601(3)	38(3)	609(3)	33(4)
550	537(8)	70(6)	562(8)	60(7)	572(6)	55(5)

Wolf	m-xylene		o-xylene		p-xylene	
T/[K]	ρ_l/[kg/m^3]	ρ_v/[kg/m^3]	ρ_l/[kg/m^3]	ρ_v/[kg/m^3]	ρ_l/[kg/m^3]	ρ_v/[kg/m^3]
375	755(2)	2.1(4)	771(2)	1.8(1)	773(2)	1.5(3)
400	731(2)	4.1(3)	747(2)	3.6(4)	750(1)	3.2(9)
425	705(4)	7(2)	722(4)	6.3(5)	727(3)	5(2)
450	679(4)	11(2)	695(2)	10(1)	700(1)	9(1)
475	647(2)	17(3)	667(2)	167(1)	673(2)	15(1)
500	614(2)	28(2)	635(3)	25(3)	643(4)	22(2)
525	578(3)	43(3)	603(4)	40(2)	610(3)	35(5)
550	535(3)	70(3)	558(3)	56(6)	570(4)	49(8)

Table S5: VLE simulation results for liquid densities (ρ_l) and vapor densities (ρ_v) of m-xylene, o-xylene, and p-xylene for different temperatures (T) obtained with the OPLS force field using the Ewald and the Wolf methods. The numbers between round brackets denote the uncertainties in the last digit.

Ewald	m-xylene		o-xylene		p-xylene	
T/[K]	ρ_l/[kg/m^3]	ρ_v/[kg/m^3]	ρ_l/[kg/m^3]	ρ_v/[kg/m^3]	ρ_l/[kg/m^3]	ρ_v/[kg/m^3]
375	780(2)	2.4(4)	796(3)	1.7(3)	775(3)	2.3(5)
400	755(3)	4.3(7)	772(2)	4(1)	750(1)	3.9(3)
425	729(2)	8.3(8)	746(3)	8(1)	726(2)	8(1)
450	701(2)	13(1)	718(1)	11(2)	696(2)	13(2)
475	670(3)	21(2)	670(1)	19(2)	667(3)	22(2)
500	636(2)	32(5)	657(2)	29(3)	634(4)	32(4)
525	601(5)	53(3)	627(5)	51(5)	600(5)	56(3)
550	555(9)	78(3)	583(5)	70(6)	554(5)	78(5)

Wolf	m-xylene		o-xylene		p-xylene	
T/[K]	ρ_l/[kg/m^3]	ρ_v/[kg/m^3]	ρ_l/[kg/m^3]	ρ_v/[kg/m^3]	ρ_l/[kg/m^3]	ρ_v/[kg/m^3]
375	778(2)	1.9(2)	796(3)	1.5(3)	775(2)	1.8(4)
400	753(4)	3.8(5)	772(1)	3.5(1)	750(2)	3.3(4)
425	728(3)	7.3(7)	745(3)	6.8(2)	724(3)	6.3(7)
450	698(3)	10(2)	717(4)	10(2)	697(2)	12(2)
475	669(4)	17(2)	689(3)	18(3)	665(3)	17(2)
500	634(3)	28(3)	656(1)	25(1)	631(5)	28(2)
525	595(4)	42(2)	615(5)	36(4)	590(7)	39(6)
550	545(13)	64(7)	571(5)	52(4)	541(4)	62(2)

Table S6: VLE simulation results for liquid densities (ρ_l) and vapor densities (ρ_v) of m-xylene, o-xylene, and p-xylene for different temperatures (T) obtained with the AUA force field using the Ewald and the Wolf methods. The numbers between round brackets denote the uncertainties in the last digit.

Ewald	m-xylene		o-xylene		p-xylene	
T/[K]	ρ_l/[kg/m^3]	ρ_v/[kg/m^3]	ρ_l/[kg/m^3]	ρ_v/[kg/m^3]	ρ_l/[kg/m^3]	ρ_v/[kg/m^3]
375	796(2)	2.1(4)	807(2)	1.9(4)	792(2)	1.1(3)
400	771(3)	3.9(4)	782(2)	2.9(5)	769(2)	3.1(8)
425	746(1)	6(1)	757(2)	6.1(6)	742(2)	5.4(9)
450	718(3)	10(1)	731(2)	8.7(3)	716(3)	10(1)
475	689(5)	16(2)	703(2)	17(2)	686(2)	16(3)
500	657(4)	24(2)	672(3)	23(3)	655(2)	24(1)
525	621(5)	38(2)	637(4)	36(3)	621(4)	40(4)
550	576(9)	54(6)	599(2)	53(3)	580(2)	60(3)

Wolf	m-xylene		o-xylene		p-xylene	
T/[K]	ρ_l/[kg/m^3]	ρ_v/[kg/m^3]	ρ_l/[kg/m^3]	ρ_v/[kg/m^3]	ρ_l/[kg/m^3]	ρ_v/[kg/m^3]
375	795(1)	1.2(4)	806(2)	1.2(4)	793(1)	1.5(2)
400	771(1)	3.2(4)	782(2)	2.7(5)	768(1)	2.7(2)
425	745(2)	5.9(6)	758(2)	4.4(3)	743(2)	5(1)
450	718(3)	8.4(7)	730(2)	9(2)	715(3)	9(2)
475	689(4)	15(2)	703(1)	15(2)	686(1)	16(2)
500	656(3)	23(2)	668(3)	18(3)	655(2)	23(2)
525	620(4)	34(3)	636(3)	33(3)	620(6)	37(3)
550	579(7)	52(3)	594(7)	47(7)	578(5)	57(1)

Table S7: Chemical potentials (μ) of m-xylene, o-xylene, and p-xylene for different temperatures (T) obtained with the TraPPE-UA force field. The subscripts l and v indicate the liquid and vapor boxes, respectively. The numbers between round brackets denote the uncertainties in the last digit.

	m-xylene		o-xylene		p-xylene	
T/[K]	μ_l/[kJ/mol]	μ_v/[kJ/mol]	μ_l/[kJ/mol]	μ_v/[kJ/mol]	μ_l/[kJ/mol]	μ_v/[kJ/mol]
375	-36.0(5)	-35.9(4)	-36.9(5)	-36.8(3)	-35.9(7)	-35.9(6)
400	-36.8(3)	-36.7(2)	-36.8(5)	-36.8(6)	-36.4(3)	-36.3(4)
425	-36.6(7)	-36.5(6)	-36.5(4)	-36.4(4)	-36.7(3)	-36.7(4)
450	-37.3(5)	-37.2(5)	-37.7(6)	-37.8(6)	-37.2(3)	-37.1(2)
475	-37.8(4)	-37.8(5)	-38.0(3)	-38.1(3)	-37.7(4)	-37.6(5)
500	-38.0(4)	-38.1(5)	-38.3(5)	-38.3(3)	-38.1(2)	-38.1(1)
525	-38.7(4)	-38.7(5)	-39.0(2)	-39.1(2)	-38.6(3)	-38.7(1)
550	-39.2(2)	-39.4(2)	-39.7(2)	-39.7(4)	-39.3(4)	-39.3(3)

Table S8: Chemical potentials (μ) of m-xylene, o-xylene, and p-xylene for different temperatures (T) obtained with the TraPPE-UA-EH force field using the Wolf and Ewald methods. The subscripts l and v indicate the liquid and vapor boxes, respectively. The numbers between round brackets denote the uncertainties in the last digit.

Ewald	m-xylene		o-xylene		p-xylene	
T/[K]	μ_l/[kJ/mol]	μ_v/[kJ/mol]	μ_l/[kJ/mol]	μ_v/[kJ/mol]	μ_l/[kJ/mol]	μ_v/[kJ/mol]
375	-35.6(4)	-35.5(5)	-35.9(2)	-35.9(2)	-36.3(7)	-36.3(6)
400	-35.8(2)	-35.7(2)	-36.2(4)	-36.1(3)	-37.1(4)	-37.0(5)
425	-36.4(2)	-36.4(3)	-37.2(8)	-37.2(7)	-36.6(4)	-36.7(3)
450	-36.6(4)	-36.6(3)	-37.0(4)	-37.1(3)	-37.7(4)	-37.8(5)
475	-37.2(3)	-37.3(3)	-37.7(2)	-37.7(2)	-38.1(3)	-38.1(4)
500	-38.1(1)	-38.0(2)	-38.3(2)	-38.3(2)	-38.5(2)	-38.6(4)
525	-38.3(4)	-38.3(3)	-39.0(3)	-39.0(2)	-39.3(2)	-39.3(3)
550	-38.9(3)	-39.0(3)	-39.5(4)	-39.5(3)	-39.8(4)	-39.8(5)

Wolf	m-xylene		o-xylene		p-xylene	
T/[K]	μ_l/[kJ/mol]	μ_v/[kJ/mol]	μ_l/[kJ/mol]	μ_v/[kJ/mol]	μ_l/[kJ/mol]	μ_v/[kJ/mol]
375	-35.5(5)	-35.4(6)	-36.0(3)	-35.9(3)	-36.5(5)	-36.4(5)
400	-35.8(1)	-35.8(2)	-36.2(4)	-36.1(4)	-36.5(7)	-36.5(6)
425	-36.2(3)	-36.2(4)	-36.7(3)	-36.6(4)	-37.2(9)	-37.2(7)
450	-36.8(3)	-36.7(4)	-37.3(4)	-37.2(5)	-37.6(6)	-37.6(5)
475	-37.6(6)	-37.5(6)	-37.6(2)	-37.7(2)	-38.0(3)	-38.0(1)
500	-37.8(3)	-37.9(3)	-38.3(3)	-38.3(2)	-38.6(4)	-38.6(1)
525	-38.6(3)	-38.5(3)	-38.8(2)	-38.7(1)	-39.2(1)	-39.2(3)
550	-39.0(1)	-39.0(2)	-39.6(3)	-39.6(1)	-39.8(4)	-39.9(4)

Table S9: Chemical potentials (μ) of m-xylene, o-xylene, and p-xylene for different temperatures (T) obtained with the OPLS force field using the Wolf and Ewald methods. The subscripts l and v indicate the liquid and vapor boxes, respectively. The numbers between round brackets denote the uncertainties in the last digit.

Ewald	m-xylene		o-xylene		p-xylene	
T/[K]	μ_{l}/[kJ/mol]	μ_{v}/[kJ/mol]	μ_{l}/[kJ/mol]	μ_{v}/[kJ/mol]	μ_{l}/[kJ/mol]	μ_{v}/[kJ/mol]
375	-35.8(5)	-35.8(6)	-36.9(4)	-36.9(4)	-35.8(7)	-35.8(6)
400	-36.4(7)	-36.3(7)	-36.7(9)	-36.7(8)	-36.6(4)	-36.6(5)
425	-36.4(2)	-36.4(2)	-36.6(3)	-36.5(4)	-36.5(4)	-36.4(5)
450	-36.9(2)	-36.9(2)	-37.5(4)	-37.5(3)	-37.0(7)	-37.1(5)
475	-37.3(5)	-37.3(4)	-37.7(3)	-37.6(3)	-37.3(2)	-37.3(4)
500	-37.9(2)	-37.8(3)	-38.2(3)	-38.2(5)	-37.9(3)	-37.9(4)
525	-38.4(2)	-38.4(2)	-38.4(2)	-38.5(1)	-38.3(3)	-38.3(2)
550	-39.0(1)	-39.2(2)	-39.3(2)	-39.4(3)	-39.1(2)	-39.0(2)

Wolf	m-xylene		o-xylene		p-xylene	
T/[K]	μ_{l}/[kJ/mol]	μ_{v}/[kJ/mol]	μ_{l}/[kJ/mol]	μ_{v}/[kJ/mol]	μ_{l}/[kJ/mol]	μ_{v}/[kJ/mol]
375	-35.8(3)	-35.7(4)	-36.3(6)	-36.3(5)	-36.1(5)	-36.0(5)
400	-36.0(4)	-36.0(4)	-36.2(3)	-36.2(4)	-36.5(5)	-36.4(4)
425	-36.2(4)	-36.1(3)	-36.4(2)	-36.4(1)	-36.6(6)	-36.5(6)
450	-37.2(4)	-37.2(5)	-37.3(5)	-37.3(3)	-36.6(3)	-36.6(4)
475	-37.6(3)	-37.5(3)	-37.4(5)	-37.4(5)	-37.6(3)	-37.6(4)
500	-37.9(3)	-37.9(3)	-38.2(5)	-38.2(4)	-37.8(1)	-37.8(3)
525	-38.6(4)	-38.6(3)	-39.0(4)	-38.9(4)	-38.7(4)	-38.7(3)
550	-39.1(4)	-39.1(2)	-39.6(4)	-39.7(4)	-39.2(2)	-39.3(2)

Table S10: Chemical potentials (μ) of m-xylene, o-xylene, and p-xylene for different temperatures (T) obtained with the AUA force field using the Wolf and Ewald methods. The subscripts l and v indicate the liquid and vapor boxes, respectively. The numbers between round brackets denote the uncertainties in the last digit.

Ewald	m-xylene		o-xylene		p-xylene	
T/[K]	μ_l/[kJ/mol]	μ_v/[kJ/mol]	μ_l/[kJ/mol]	μ_v/[kJ/mol]	μ_l/[kJ/mol]	μ_v/[kJ/mol]
375	-35.5(5)	-35.4(6)	-35.8(5)	-35.7(6)	-37.5(7)	-37.3(6)
400	-35.9(5)	-35.9(5)	-36.8(5)	-36.8(5)	-36.6(7)	-36.5(8)
425	-37.0(4)	-36.9(5)	-36.6(3)	-36.6(4)	-37.2(4)	-37.1(4)
450	-37.1(3)	-37.1(3)	-37.6(1)	-37.6(2)	-37.1(3)	-37.1(2)
475	-37.5(3)	-37.6(3)	-37.4(5)	-37.4(4)	-37.6(4)	-37.6(4)
500	-38.2(2)	-38.2(2)	-38.3(5)	-38.3(4)	-38.2(2)	-38.2(2)
525	-38.7(2)	-38.7(1)	-38.8(3)	-38.8(1)	-38.5(5)	-38.5(2)
550	-39.5(3)	-39.5(2)	-39.5(2)	-39.5(1)	-39.2(3)	-39.2(2)

Wolf	m-xylene		o-xylene		p-xylene	
T/[K]	μ_l/[kJ/mol]	μ_v/[kJ/mol]	μ_l/[kJ/mol]	μ_v/[kJ/mol]	μ_l/[kJ/mol]	μ_v/[kJ/mol]
375	-37.2(9)	-37.2(9)	-37.1(6)	-37.1(7)	-36.3(5)	-36.4(5)
400	-36.3(3)	-36.5(3)	-37.1(7)	-37.2(7)	-37.0(3)	-37.1(3)
425	-36.7(3)	-36.8(3)	-37.6(3)	-37.8(1)	-37.3(6)	-37.4(4)
450	-37.6(3)	-37.7(3)	-37.5(5)	-37.7(5)	-37.5(5)	-37.7(4)
475	-37.9(4)	-38.0(4)	-37.9(4)	-38.1(4)	-37.7(4)	-37.9(3)
500	-38.3(2)	-38.5(2)	-39.0(5)	-39.1(4)	-38.5(2)	-38.7(4)
525	-38.9(1)	-39.1(2)	-39.0(3)	-39.1(4)	-38.9(3)	-39.0(4)
550	-39.7(2)	-39.8(3)	-39.9(4)	-40.0(4)	-39.3(4)	-39.5(5)

Table S11: VLE phase composition for the p-xylene/o-xylene binary mixture at 6.66 kPa for each force field and experimental data[8]. (E) and (W) denote the use of the Ewald and the Wolf methods, respectively. x_{pX} is the mole fraction of pX in the liquid phase. y_{pX} is the mole fraction of pX in the vapor phase. The numbers between round brackets denote the uncertainties in the last digit.

	Experimental[8]		TraPPE-UA		TraPPE-UA-EH (E)		TraPPE-UA-EH (W)	
T/[K]	x_{pX}	y_{pX}	x_{pX}	y_{pX}	x_{pX}	y_{pX}	x_{pX}	y_{pX}
332.55	0.948(1)	0.959(1)	0.960(5)	0.841(44)	0.961(6)	0.838(55)	0.955(5)	0.882(54)
332.85	0.895(1)	0.915(1)	0.904(4)	0.821(37)	0.902(3)	0.845(28)	0.896(2)	0.906(26)
333.25	0.815(1)	0.849(1)	0.821(6)	0.778(59)	0.825(2)	0.720(37)	0.814(2)	0.819(25)
333.65	0.738(1)	0.780(1)	0.749(4)	0.678(35)	0.743(3)	0.713(39)	0.740(2)	0.754(27)
334.45	0.577(1)	0.633(1)	0.577(2)	0.616(13)	0.574(3)	0.657(31)	0.576(3)	0.632(32)
334.85	0.497(1)	0.555(1)	0.497(3)	0.544(27)	0.497(2)	0.533(17)	0.499(4)	0.527(37)
335.25	0.420(1)	0.477(1)	0.418(3)	0.470(22)	0.421(6)	0.459(56)	0.413(2)	0.535(21)
336.15	0.263(1)	0.310(1)	0.237(4)	0.393(25)	0.251(4)	0.249(39)	0.247(2)	0.290(25)
336.55	0.182(1)	0.219(1)	0.170(3)	0.296(22)	0.181(3)	0.228(29)	0.180(4)	0.236(40)
337.05	0.100(1)	0.125(1)	0.079(3)	0.284(20)	0.093(4)	0.186(34)	0.091(2)	0.200(20)

	OPLS (E)		OPLS (W)		AUA(E)		AUA (W)	
T/[K]	x_{pX}	y_{pX}	x_{pX}	y_{pX}	x_{pX}	y_{pX}	x_{pX}	y_{pX}
332.55	0.960(11)	0.841(97)	0.952(2)	0.916(22)	0.955(2)	0.884(16)	0.951(5)	0.924(62)
332.85	0.907(7)	0.813(58)	0.898(3)	0.889(39)	0.902(4)	0.844(41)	0.895(2)	0.921(20)
333.25	0.832(11)	0.702(73)	0.822(5)	0.761(53)	0.820(3)	0.791(33)	0.816(3)	0.831(37)
333.65	0.747(8)	0.691(67)	0.740(2)	0.753(17)	0.745(2)	0.717(34)	0.732(2)	0.806(43)
334.45	0.575(5)	0.633(48)	0.579(2)	0.601(22)	0.581(3)	0.579(24)	0.579(4)	0.610(42)
334.85	0.491(7)	0.593(59)	0.494(3)	0.563(27)	0.492(2)	0.599(20)	0.496(3)	0.566(38)
335.25	0.421(6)	0.454(50)	0.422(5)	0.444(52)	0.418(1)	0.473(10)	0.421(2)	0.465(29)
336.15	0.239(5)	0.358(41)	0.241(2)	0.353(17)	0.237(3)	0.378(30)	0.249(3)	0.276(36)
336.55	0.175(6)	0.278(47)	0.174(3)	0.287(37)	0.176(4)	0.276(32)	0.179(3)	0.255(28)
337.05	0.084(10)	0.247(75)	0.097(2)	0.158(18)	0.082(4)	0.267(25)	0.093(5)	0.204(53)

Table S12: Excess chemical potential ($\mu^{e}{}_{pX}$) of p-xylene in the liquid phase of the p-xylene/o-xylene binary mixture at 6.66 kPa for different temperatures (T) and different force fields. (E) and (W) denote the use of the Ewald and the Wolf methods, respectively. The numbers between round brackets denote the uncertainties in the last digit.

	TraPPE-UA	TraPPE-UA-EH	
T/[K]	$\mu^{e}{}_{pX}$/[kJ/mol]	$\mu^{e}{}_{pX}$/[kJ/mol] (E)	$\mu^{e}{}_{pX}$/[kJ/mol] (W)
332.55	-22.3(1)	-22.6(2)	-22.3(3)
332.85	-22.4(2)	-22.7(2)	-22.3(2)
333.25	-22.4(1)	-22.7(1)	-22.4(2)
333.65	-22.5(2)	-22.7(1)	-22.5(4)
334.45	-22.5(3)	-22.7(2)	-22.5(1)
334.85	-22.6(2)	-22.9(3)	-22.5(1)
335.25	-22.6(2)	-22.8(2)	-22.6(2)
336.15	-22.6(1)	-22.9(4)	-22.6(1)
336.55	-22.6(2)	-22.9(1)	-22.6(3)
337.05	-22.8(2)	-23.1(1)	-22.6(3)
337.25	-22.8(1)	-23.0(3)	-22.7(5)

	OPLS		AUA	
T/[K]	$\mu^{e}{}_{pX}$/[kJ/mol] (E)	$\mu^{e}{}_{pX}$/[kJ/mol] (W)	$\mu^{e}{}_{pX}$/[kJ/mol] (E)	$\mu^{e}{}_{pX}$/[kJ/mol] (W)
332.55	-23.5(6)	-22.3(7)	-22.3(3)	-22.3(2)
332.85	-23.6(9)	-22.4(6)	-22.6(2)	-22.3(3)
333.25	-23.6(7)	-22.4(5)	-22.5(5)	-22.2(3)
333.65	-23.7(9)	-22.3(6)	-22.6(3)	-22.4(4)
334.45	-23.8(10)	-22.5(8)	-22.6(3)	-22.5(3)
334.85	-23.8(7)	-22.5(7)	-22.7(4)	-22.4(1)
335.25	-23.8(8)	-22.6(8)	-22.6(2)	-22.4(1)
336.15	-23.8(6)	-22.7(7)	-22.7(2)	-22.5(2)
336.55	-24.0(9)	-22.7(5)	-22.8(1)	-22.6(2)
337.05	-23.9(8)	-22.7(8)	-22.8(1)	-22.6(3)
337.25	-24.1(8)	-22.7(6)	-22.9(2)	-23.0(1)

Table S13: VLE phase composition for the p-xylene/o-xylene binary mixture at 81.3 kPa for each force field using the Ewald method, and experimental data[9]. x_{pX} is the mole fraction of pX in the liquid phase. y_{pX} is the mole fraction of pX in the vapor phase. The numbers between round brackets denote the uncertainties in the last digit.

	Experimental[9]		TraPPE-UA		TraPPE-UA-EH	
T/[K]	x_{pX}	y_{pX}	x_{pX}	y_{pX}	x_{pX}	y_{pX}
401.65	0.870	0.901	0.878(10)	0.828(73)	0.891(5)	0.750(30)
402.20	0.732	0.780	0.719(5)	0.845(25)	0.753(5)	0.602(32)
402.95	0.571	0.627	0.564(9)	0.638(53)	0.579(9)	0.548(63)
403.65	0.442	0.491	0.427(7)	0.582(47)	0.441(9)	0.469(65)
404.90	0.232	0.258	0.198(4)	0.470(33)	0.230(5)	0.257(28)
405.25	0.148	0.166	0.118(5)	0.380(43)	0.126(11)	0.280(47)
405.50	0.051	0.057	0.003(1)	0.290(19)	0.039(8)	0.139(54)

	OPLS		AUA	
T/[K]	x_{pX}	y_{pX}	x_{pX}	y_{pX}
401.65	0.923(27)	0.669(95)	0.887(6)	0.759(47)
402.20	0.755(17)	0.647(78)	0.753(4)	0.631(20)
402.95	0.580(6)	0.554(26)	0.574(4)	0.582(35)
403.65	0.416(18)	0.553(57)	0.444(3)	0.451(15)
404.90	0.169(31)	0.471(90)	0.186(7)	0.510(43)
405.25	0.082(14)	0.405(47)	0.102(9)	0.432(50)
405.50	0.004(7)	0.251(26)	0.028(7)	0.212(36)

References

(1) Wick, C. D.; Martin, M. G.; Siepmann, J. I. Transferable Potentials for Phase Equilibria. 4. United-Atom Description of Linear and Branched Alkenes and Alkylbenzenes. *Journal of Physical Chemistry B* **2000**, *104*, 8008–8016.

(2) Rai, N.; Siepmann, J. I. Transferable Potentials for Phase Equilibria. 9. Explicit Hydrogen Description of Benzene and Five-Membered and Six-Membered Heterocyclic Aromatic Compounds. *Journal of Physical Chemistry B* **2007**, *111*, 10790–10799.

(3) Jorgensen, W. L.; Laird, E. R.; Nguyen, T. B.; Tirado-Rives, J. Monte Carlo simulations of pure liquid substituted benzenes with OPLS potential functions. *Journal of Computational Chemistry* **1993**, *14*, 206–215.

(4) Jorgensen, W. L.; Maxwell, D. S.; Tirado-Rives, J. Development and Testing of the OPLS All-Atom Force Field on Conformational Energetics and Properties of Organic Liquids. *Journal of the American Chemical Society* **1996**, *118*, 11225–11236.

(5) Nieto-Draghi, C.; Bonnaud, P.; Ungerer, P. Anisotropic United Atom Model Including the Electrostatic Interactions of Methylbenzenes. I. Thermodynamic and Structural Properties. *Journal of Physical Chemistry C* **2007**, *111*, 15686–15699.

(6) Nieto-Draghi, C.; Bonnaud, P.; Ungerer, P. Anisotropic United Atom Model Including the Electrostatic Interactions of Methylbenzenes. II. Transport Properties. *Journal of Physical Chemistry C* **2007**, *111*, 15942–15951.

(7) Dubbeldam, D.; Calero, S.; Vlugt, T. J. H. iRASPA: GPU-accelerated visualization software for materials scientists. *Molecular Simulation* **2018**, *44*, 653–676.

(8) Llopis, F. J.; Monton, J. B. Isobaric vapor-liquid equilibria of p-xylene + o-xylene and m-xylene + o-xylene systems at 6.66 and 26.66 kPa. *Journal of Chemical & Engineering Data* **1994**, *39*, 53–55.

(9) Parvez, M.; Singh, G.; Tyagi, S.; Kumar, S.; Khan, S. Experimental determination of vapour-liquid equilibrium data for the binary mixtures P-Xylene and O-Xylene at 81.3 kPa. *Journal of Scientific and Technical Advancements* **2015**, *1*, 263–265.